Chinese Chemical Letters 34 (2023) 107368

Contents lists available at ScienceDirect

Chinese Chemical Letters

journal homepage: www.elsevier.com/locate/cclet

Construction of novel cluster-based MOF as multifunctional platform for CO_2 catalytic transformation and dye selective adsorption

Xiuling Zhang[a,b,1], Yongzheng Zhang[a,1], Wenfeng Zhou[a,b], Huiling Liu[a], Dashuai Zhang[a,b,c,*], Hui Hu[a], Chao Lv[a], Suijun Liu[c,*], Longlong Geng[a,b,*]

[a] College of Chemistry and Chemical Engineering, Dezhou University, Dezhou 253023, China
[b] School of Chemistry and Chemical Engineering, Shandong University of Technology, Zibo 255000, China
[c] Jiangxi Provincial Key Laboratory of Functional Molecular Materials Chemistry, School of Chemistry and Chemical Engineering, Jiangxi University of Science and Technology, Ganzhou 341000, China

ARTICLE INFO

Article history:
Received 17 January 2022
Revised 5 March 2022
Accepted 21 March 2022
Available online 25 March 2022

Keywords:
Metal–organic frameworks
Metal cluster
Catalysis
CO_2 cycloaddition
Dye separation

ABSTRACT

Synthetic conditions and ligands are the key structural defining factors of metal–organic frameworks (MOFs). Therefore, reasonable optimization of these aspects is considered to be an effective means for designing materials with novel structures and target functions. Herein, two novel Co(II)-based MOFs, namely $[Co(HL)(dibp)]_n$ (**HL-8**) and $\{[Co_2(L)(OH)(dibp)]\cdot DMA\}_n$ (**HL-9**) (H_3L = 2′,6′-dimethyl-[1,1′-biphenyl]-3,4′,5-tricarboxylic acid; dibp = 4,4′-di(1*H*-imidazol-1-yl)-1,1′-biphenyl]), have been hydrothermally synthesized and structurally characterized. **HL-8** crystallizes in the orthorhombic system ($Pna2_1$) with a grid layer structure, while **HL-9** crystallizes in the monoclinic $P2_1/n$ space group assembled through $Co_4(OH)_2$ clusters with organic ligands. Remarkably, benefiting from the finite cage-like structure, **HL-9** exhibited enhanced performance in carbon dioxide (CO_2) adsorption/catalytic transformation and excellent size selectivity during dye molecular adsorption process.

Metal–organic frameworks (MOFs) are an emerging class of porous crystalline materials constructed from inorganic nodes (metal ions/clusters) with organic linkers through coordination bonds [1–3]. Due to their unique properties of diverse composition, large surface area, and ease of functionalization, MOFs have interesting applications in gas adsorption and separation, energy storage, molecular sensing, optoelectronics, heterogeneous catalysis, and so on [4–9].

In recent years, environmental pollution caused by the consumption of fossil energy and emissions from the chemical industry has become a global concern [10,11]. For example, excessive emissions of greenhouse gases, especially carbon dioxide (CO_2), are considered to be the main reason of the extreme climate in recent years, such as melting glaciers and global warming [12–16]. In addition, various toxic organic dyes or intermediates produced by the chemical industry are commonly detected in the groundwater and arable land, with negative effects on human health through the biological chain [17–19]. To ameliorate these issues, assorted MOF-based materials with highly porous structures and functional groups have been designed and prepared, and some success has been achieved through absorption, conversion, or degradation [20–22]. A key factor determining the performance of MOFs during their usage is the appropriate interaction between waste molecules and metal sites in the framework [23,24]. In particular, MOFs with unsaturated metal sites have shown excellent performance in the field of adsorption and catalysis due to the unique structural and electronic characteristics [25–29]. Unfortunately, the metal nodes in most MOFs structures are usually blocked by organic linkers, leaving no coordination active sites available for the binding and activation of substrates, which limits their practical application.

Fortunately, the high structural designability and easy functionalization of MOFs make it an ideal platform in a variety of applications [30,31]. From the structural viewpoint of MOFs, metal clusters can provide more coordination sites during the organization of the framework and therefore generate unsaturated metal sites [32–34], although it is challengeable due to the flexible coordination modes. In this work, two new Co-based MOFs were solvothermal synthesized and structural characterized. Interestingly, the same metal nodes and organic ligands assembled but different solvents gave two MOFs with distinct topologies. Their potential usage in the CO_2 selective adsorption and chemical transformation as well as dye adsorption was evaluated in detail.

* Corresponding authors.
E-mail addresses: dashuai_74@163.com (D. Zhang), sjliu@jxust.edu.cn (S. Liu), llgeng@126.com (L. Geng).
[1] These authors contributed equally to this work.

https://doi.org/10.1016/j.cclet.2022.03.091
1001-8417/

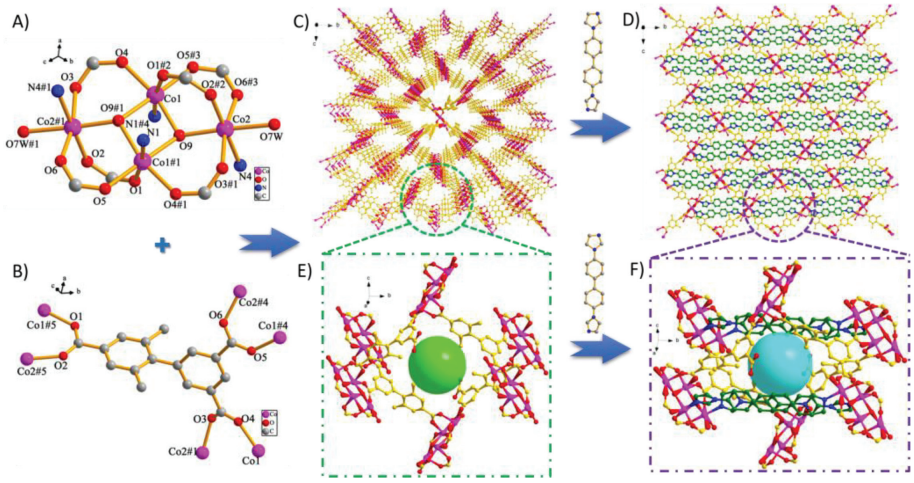

Fig. 1. Structures of **HL-9**: (A) The Co_4 cluster formed by μ_3-OH and -COO^- groups. (B) The coordination mode of the -COO^- groups in L^{3-} ligands. (C) The porous framework with one-dimensional (1D) rhombic channels formed by the connection of Co_4 cluster and L^{3-} ligands. (D) The final structures of **HL-9** with dibp ligands splitting the rhombic channels. (E,F) Formation of the cage structures inside the framework.

Single-crystal diffraction analysis reveals that **HL-8** crystallizes in the orthorhombic system, space group $Pna2_1$ (Table S1 in Supporting information). As exhibited in Fig. S1a (Supporting information), there exists one crystallographically independent Co(II) center, which is coordinated by four carboxylate O atoms from two L^{3-} ligands and two imidazole N atoms from two dibp ligands, showing a tetrahedral geometry. From Figs. S1b–d (Supporting information), each HL^{2-} ligand as a μ_2-bridging linker with μ_2-η^1:η^1 coordination mode connects Co(II) forming a 1D chain structure and each didp ligand linking two Co(II) also from another chain structure. Finally, the two kinds of chains weave together to generate the final 3D framework of **HL-8** (Fig. S1e in Supporting information). Due to the stemming of the uncoordinated -COOH groups, **HL-8** reveals a low porosity, and the solvent accessible volume of **HL-8** is 306.1 $Å^3$ per 3275.6 $Å^3$ unit cell volume (9.3% of the total crystal volume). Moreover, if the Co(II) center is viewed as 4-connected node, the structure of **HL-8** can be simplified as 4-connected sqc5 type topology with the point symbol $\{6^5{\cdot}8\}$ (Fig. S1f in Supporting information).

Different from **HL-8**, **HL-9** crystallizes in the monoclinic $P2_1/n$ space group (Table S1) and has a novel three-dimensional (3D) porous structure. In the structure, there exist two crystallographically independent Co atoms (Fig. S1a). Co1 is coordinated by three O atoms from carboxylates of different L^{3-} ligands, two μ_3-OH entities, one N atom from dibp ligand, while Co2 is coordinated by three O atoms from carboxylates of different L^{3-} ligands, one μ_3-OH entities, one N atom from dibp ligand and one O from a terminal H_2O. Two μ_3-OH and six -COO^- groups connecting four Co atoms form a $Co_4(OH)_2(COO)_6$ cluster (Fig. 1A), and each L^{3-} ligand in a μ_6-η^2:η^2:η^2 coordination manner links three Co_4 clusters forming a 3D framework with 1D rhombic channels along *a* axis (Figs. 1B and C). Each dibp ligand connects to two Co_4 clusters and inserts to the rhombic channels generating the final framework structures of **HL-9** (Fig. 1D) with a total solvent-accessible volume of 34.2% estimated by PLATON [34]. Interestingly, due to the insertion of dibp ligands, the framework of **HL-9** is split into finite cage-like voids (Figs. 1E and F). Topologically, L^{3-} ligand can be seen as a 3-connected linker and Co_4 cluster as an 8-connected node, the 3D framework of **HL-9** can thus be simplified as a novel (3,8)-connected network with the point symbol of $\{4{\cdot}5^2\}_2\{4^2{\cdot}5^{10}{\cdot}6^{12}{\cdot}7{\cdot}8^3\}$ (Fig. S2b in Supporting information).

The synthesized samples were further characterized by powder X-ray diffraction (PXRD) and thermogravimetric analysis (TG) to confirm the purity of crystal phases as well as solvent stability in potential applications. The characteristic peaks of PXRD patterns for both **HL-8** and **HL-9** match well with corresponding simulated ones, as demonstrated in Fig. S3 (Supporting information), confirming the high purity of the crystals. In addition, the position and intensity of each peak were almost unchanged after soaking both compounds in water and different dye solvents, proving their crystallinity was maintained. The high chemical stability is of vital importance for their practical usage [35,36]. TG curves under nitrogen atmosphere indicated that **HL-8** and **HL-9** can be thermal stable up to 366 °C and 405 °C (Fig. S4 in Supporting information), respectively, confirming their excellent thermal stabilities and wide application potential under mild conditions.

In view of the interesting gas adsorption behavior of MOF-based materials, the gas adsorption properties of the as-synthesized compounds were investigated. As shown in Fig. S5A (Supporting information), negligible adsorption for nitrogen, methane, and carbon dioxide was obtained over **HL-8**, which should be caused by its low porosity and solvent accessible volume. As for **HL-9**, inferior nitrogen and methane uptake is also observed (Fig. S5B in Supporting information). However, as displayed in Fig. 2A, **HL-9** exhibited superior CO_2 adsorption behavior under low pressure (1 atm). The amount of CO_2 uptake on **HL-9** is 72.7 cm^3/g, which is 52 times that of **HL-8** (1.4 cm^3/g). The calculated isosteric heats of CO_2 adsorption (Q_{st}) at zero coverage was calculated in a range of 27.2−36.5 kJ/mol, by fitting the CO_2 isotherms at 273 and 298 K with the virial method, which reflects a good interaction between the CO_2 molecular and HL-9 (Fig. S6 in Supporting information). Based on the results in previous works [37,38], the unique CO_2 adsorption behavior on **HL-9** should be correlated to the existence of Co_4 clusters and cage-like voids in the framework, which may generate interaction with CO_2 molecules and therefore result in high adsorption performances.

Taking advantage of the excellent CO_2 adsorption property and relatively high thermal/solution stability, the potential usage of the obtained compounds in CO_2 catalytic transformation was further explored. Till now, a variety of CO_2 harvesting and chemical fixation methods have been explored by chemists and some successes have been achieved in converting CO_2 into valuable energy and/or chemicals [39]. Among the chemical conversion routes, the synthesis of value-added epoxy carbonates through cycloaddition of CO_2 with epoxides was widely studied by researchers due to its high reactivity under mild conditions as well as the wide usage of the

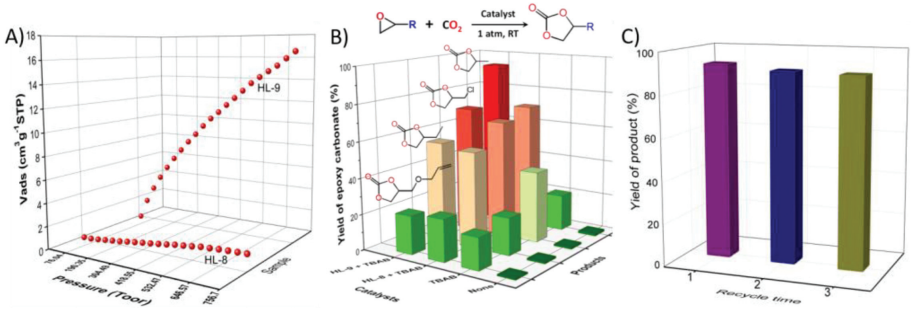

Fig. 2. (A) CO_2 sorption isotherms of **HL-8** and **HL-9** at 273 K. (B) Catalytic performance in CO_2 cycloaddition with epoxides over **HL-8** and **HL-9** and (C) recyclability of **HL-9** in CO_2 cycloaddition process.

final products as solvents, organic intermediates, and electrolytes [37,40–42]. The efficient adsorption and subsequent activation of CO_2 is the key to the above transformation.

Fig. 2B and Table S3 (Supporting information) summarized the catalytic performance of the different catalysts in cycloaddition of CO_2 with various epoxides. No product was obtained in the absence of any catalysts or with only ligands of **HL-9** as catalyst. Traditional tetrabutylammonium bromide (TBAB) catalyst also exhibited inferior activity with low epoxy carbonates yields, which was in agreement with the previous literature results [42,43]. Interestingly, the addition of the Co-containing compounds greatly improves the conversion of reactants under the same conditions, confirming the synergism of the compounds and TBAB in the catalytic process. The yield of propylene carbonate is 93.2% and 70.1% for **HL-9** and **HL-8**, respectively, confirming the superior performance of **HL-9** under mild conditions. This value is comparable to most literature-reported MOFs (Table S3). Notable, a 91.7% yield of propylene carbonate was also obtained when using homogeneous $Co(NO_3)_2$ as a catalyst, confirming the Co species is the main active site for CO_2 catalytic transformation. In view of the recovery and reuse of catalysts, the heterogeneous nature of **HL-9** is advantageous for practical application.

In addition, **HL-9** also exhibited size-selective catalytic behavior in the title reaction. As shown in Fig. 2B, a decrease in the yield of epoxy carbonate was observed when we increase the molecular size of epoxides substrates (the yield is 93.2%, 70.7%, 55.8%, and 21.3% for 4-methyl-1,3-dioxolan-2-one, 4-(chloromethyl)-1,3-dioxolan-2-one, 4-ethyl-1,3-dioxolan-2-one and 4-((allyloxy)methyl)-1,3-dioxolan-2-one, respectively), which should be correlated with the limited diffusion of larger epoxides in the finite cage-like voids and channels of the framework . Additionally, cyclic catalysis of **HL-9** maintained a substrate yield higher than 90% in 3 cycles (Fig. 2C), confirming its usage potential in practical applications.

Inspired by the unique size-selective behavior of **HL-9** in catalytic transformation, the dye selective capture ability was also evaluated using three selected dyes with different sizes: methyl orange (MO), methylene blue (MB), and rhodamine B (RhB). Similar to gas adsorption results, as shown in Fig. 3A and Fig. S7 (Supporting information), **HL-8** displayed neglected adsorption for all dyes. In contrast, as displayed in Fig. 3B, the orange solution of MO faded to colorless in only 35 min with the addition of **HL-9** under same conditions. The significant decrease in color intensity was consistent with the UV-vis spectroscopy results, confirming its outstanding performance in rapid adsorption of MO. The saturated capacity and apparent rate constants (k) of MO adsorption over **HL-9** were 72.4 mg/g and 44.0×10^{-3} min^{-1}, respectively (Fig. S8 in Supporting information). In addition, we also investigated the recyclability of **HL-9** in MO adsorption. It is interesting that, as shown in Fig. 3C, **HL-9** could be regenerated by releasing MO in

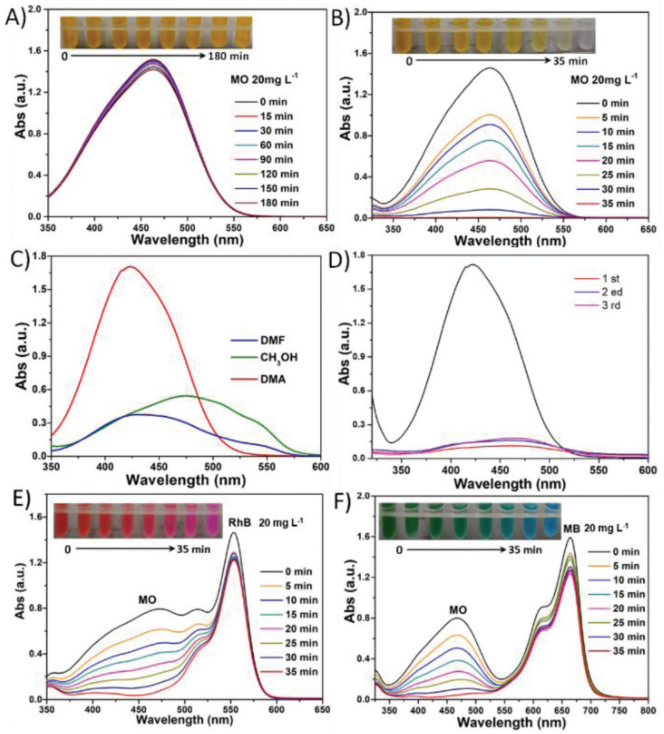

Fig. 3. Adsorption performance and color changes during adsorption of MO in the presence of (A) **HL-8** and (B) **HL-9**. (C) The UV-vis spectra of MO solution desorbed in different solvents and (D) reusability of MO adsorption over **HL-9**. MO selective adsorption performance from the mixture solution of (E) MO + RhB and (F) MO + MB.

N,*N*-dimethylacetamide (DMA) solution and reused at least three times with >95% MO adsorption efficiency (Fig. 3D). The shift in the position of the absorption peak of MO is caused by the different solvents. Besides, the PXRD patterns of RhB@**HL-9**, MB@**HL-9**, and MO-released **HL-9** after the 3rd cycle still remained the same as the as-synthesized samples (Fig. S3B in Supporting information), confirming its high stability during the adsorption process.

As for RhB and MB solution, only a slight change in color and UV-vis absorbance was observed after adding **HL-9** for 180 min (Fig. S9 in Supporting information). By comparing the open sizes of the cage-like voids of **HL-9** and the molecular sizes of MO and RhB, it is suitable for **HL-9** to adsorb and sieve MO molecule with smaller size and narrower shape than RhB (Fig. S10 in Supporting information). The above results unveiled its potential usage in selective adsorption of MO from the mixture of other dye solutions. Therefore, the competitive adsorption experiments over **HL-9** were

further performed. As shown in the inset of Figs. 3E and F, the colors rapidly changed from pink for MO + RhB to purple for RhB, and from light green for MO + MB to green for MB, respectively, after immersion of **HL-9** in the mixed dye solutions. Correspondingly, all UV-vis spectra revealed that the absorption peaks of MO decreased and gradually disappeared within 35 min without obvious change in the absorbance of RhB or MB. The outstanding absorption performance of **HL-9** highlights its potential application for size-selective separation towards the MO dyes in wastewater.

In summary, two new Co-containing MOFs were synthesized with high thermal/solution stability. Benefited from the Co_4 cluster nodes and suitable pore in the framework of **HL-9**, superior performance and interesting size selectivity were achieved in the applications of CO_2 adsorption/catalytic transformation and dye molecular adsorption. This work underlines the importance of parameter regulation during MOF synthesis, which may be a promising direction for the construction of novel MOFs with multifunctional performance.

Declaration of competing interest

The authors declare that they have no known competing financial interests or personal relationships that could have appeared to influence the work reported in this paper.

Acknowledgments

This work was supported by the National Natural Science Foundation of China (Nos. 21902022, 21601028, 81903501 and 22061019), Qingchuang Science and Technology Plan of Shandong Province (No. 2021KJ054), the Natural Science Foundation of Shandong Province (Nos. ZR2018LB018, ZR2019QB026 and ZR2020KB014) and Scientific Research Foundation of Dezhou University (Nos. 30101905, 30102708 and 30102701).

Supplementary materials

Supplementary material associated with this article can be found, in the online version, at doi:10.1016/j.cclet.2022.03.091.

References

[1] H. Furukawa, K.E. Cordova, M. O'Keeffe, O.M. Yaghi, Science 341 (2013) 1230444.
[2] X.J. Kong, J.R. Li, Engineering 7 (2021) 1115–1139.
[3] G. Huang, L. Yang, Q. Yin, et al., Angew. Chem. Int. Ed. 59 (2020) 4385–4390.
[4] L. Li, Z.B. Fang, W. Deng, et al., CCS Chem. 3 (2021) 2839–2849.
[5] Y. Zhou, L. Qin, M.K. Wu, L. Han, Cryst. Growth Des. 18 (2018) 5738–5744.
[6] F. Bi, X. Zhang, J. Chen, Y. Yang, Y. Wang, Appl. Catal. B: Environ. 269 (2020) 118767.
[7] D.S. Zhang, Q. Gao, Z. Chang, et al., Adv. Mater. 30 (2018) 1804715.
[8] J.Q. Liu, Z.D. Luo, Y. Pan, et al., Coord. Chem. Rev. 406 (2020) 213145.
[9] W. Du, Y.L. Bai, Z. Yang, et al., Chin. Chem. Lett. 31 (2020) 2309–2313.
[10] L. He, M.X. Li, F. Chen, et al., J. Hazard. Mater. 417 (2021) 126113.
[11] J. He, Y. Xu, Z. Xiong, et al., Chemosphere 256 (2020) 127056.
[12] H. Hu, D. Zhang, H. Liu, et al., Chin. Chem. Lett. 32 (2021) 557–560.
[13] B. Han, X. Ou, Z. Deng, et al., Angew. Chem. Int. Ed. 57 (2018) 16811–16815.
[14] Y. Wang, Y. Pu, D. Yuan, et al., ACS App. Mater. Interfaces 11 (2019) 44058–44068.
[15] X. Zhang, Y. Jin, G. Wang, et al., J. Solid State Chem. 296 (2021) 121979.
[16] G. Si, X. Kong, T. He, et al., Chin. Chem. Lett. 32 (2021) 918–922.
[17] H. Bi, Z. Yin, X. Cao, et al., Adv. Mater. 25 (2013) 5916–5921.
[18] L. Geng, G. Li, X. Zhang, et al., J. Solid State Chem. 296 (2021) 121960.
[19] Q. Wei, B.D. Ge, J. Zhang, et al., Chem. Asian J. 14 (2019) 269–277.
[20] Y. Peng, Y. Li, Y. Ban, et al., Science 346 (2014) 1356–1359.
[21] L. Cao, T. Wang, C. Wang, Chin. J. Chem. 36 (2018) 754–764.
[22] A.X. Tian, M.L. Yang, Y.B. Fu, J. Ying, X.L. Wang, Inorg. Chem. 58 (2019) 4190–4200.
[23] X. Zhang, H. Cheng, H. Zhang, Adv. Mater. 29 (2017) 1701704.
[24] X. Wang, T. Zhang, Y. Li, et al., Inorg. Chem. 59 (2020) 17583–17590.
[25] A. Liu, X. Peng, Q. Jin, et al., ACS Appl. Mater. Interfaces 11 (2019) 4686–4700.
[26] M. Položij, M. Rubeš, J. Čejka, P. Nachtigall, ChemCatChem 6 (2014) 2821–2824.
[27] S. Aslam, J. Zeng, F. Subhan, et al., J. Colloid Interface Sci. 505 (2017) 186–195.
[28] L. Geng, W. Zhou, X. Wang, et al., J. Alloy. Compd. 888 (2021) 161494.
[29] R. Mohammadian, M.K. Alavijeh, N. Kamyar, M.M. Amini, A. Shaabani, Polyhedron 156 (2018) 174–187.
[30] L. Jiao, J. Wang, H.L. Jiang, Acc. Mater. Res. 2 (2021) 327–339.
[31] C. Gu, J. Li, G. Yang, et al., Chin. Chem. Lett. 31 (2020) 2263–2267.
[32] M. Peng, C. Dong, R. Gao, et al., ACS Cent. Sci. 7 (2021) 262–273.
[33] Y. Bai, Y. Dou, L.H. Xie, et al., Chem. Soc. Rev. 45 (2016) 2327–2367.
[34] X. Zhang, Y.Z. Zhang, Y.Q. Jin, et al., Inorg. Chem. 59 (2020) 11728–11735.
[35] Y.Z. Zhang, T. He, X.J. Kong, et al., ACS Mater. Lett. 1 (2019) 20–24.
[36] H.Z. Li, D.Y. Du, Y. Sun, F. Wang, J. Zhang, Dalton Trans. 49 (2020) 4690–4693.
[37] J. Li, W.J. Li, S.C. Xu, et al., Inorg. Chem. Commun. 106 (2019) 70–75.
[38] R. Dalapati, B. Sakthivel, A. Dhakshinamoorthy, et al., CrystEngComm 18 (2016) 7855–7864.
[39] W.G. Cui, G.Y. Zhang, T.L. Hu, X.H. Bu, Coord. Chem. Rev. 387 (2019) 79–120.
[40] H. Chen, T. Hu, L. Fan, X. Zhang, Inorg. Chem. 60 (2021) 1028–1036.
[41] Y.J. Chen, X. Huang, Y. Chen, et al., CCS Chem. 1 (2019) 561–570.
[42] X. Zhang, R.H. Zhang, H. Hu, et al., Dalton Trans. 49 (2020) 2058–2062.
[43] J.J. Lv, F.L. Cao, M.L. Wang, et al., Polyhedron 195 (2021) 114982.